Light-Induced Activation of Forbidden Exciton Transition in Strongly Confined Perovskite Quantum

Dots

Daniel Rossi¹, Hua Wang², Yitong Dong¹, Tian Qiao¹, Xiaofeng Qian² and Dong Hee Son¹²³

Department of Chemistry, Texas A&M University, College Station, Texas 77843, USA

²Department of Materials Science and Engineering, Texas A&M University, College Station,
Texas 77843, USA

³Center for Nanomedicine, Institute for Basic Science (IBS), Seoul 03722, Republic of Korea

KEYWORDS.

perovskite. quantum dots. forbidden exciton transition. polaron. symmetry breaking

ABSTRACT

We report the strong light-induced activation of forbidden exciton transition in CsPbBr, perovskite quantum dots mediated by the symmetry-breaking polaron that modifies the optical selection rule of the confined exciton transition. The activated forbidden transition results in an intense pump-induced absorption in the transient absorption spectra above the bandgap, where the original parity-forbidden transition was located. In contrast to many other semiconductor quantum dots, photoexcitation of exciton in CsPbBr, quantum dots creates a sufficiently large perturbation *via* lattice-distorting polaron, which turns on the formally forbidden transition. Compared to the bulk or weakly confined CsPbBr, the activation of the forbidden transition in strongly confined quantum dots is much more prominent due to the stronger influence of the polaron on exciton transitions in the confined space. This nonlinear optical property highlights the intimate coupling of the photoexcited charge carriers with the lattice in the CsPbBr, quantum dots, allowing access to the forbidden exciton transitions with light.

Semiconducting lead halide perovskite nanomaterials with intense photoluminescence (PL), facile chemical tuning of PL energy and long carrier diffusion lengths are extensively studied as the next generation materials for photonic and photovoltaic applications. In particular, the colloidal nanocrystals of cesium lead halide (CsPbX₃) have attracted much attention as a potentially superior alternative to various other colloidal quantum dots (QDs) used as the source of photons and charge carriers. However, much of the research has focused on the relatively large CsPbX₃ nanocrystals without strong and controllable quantum confinement of the exciton. The properties of the confined exciton and its interaction with other degrees of freedom in CsPbX₃ QDs have been rarely explored, despite its importance in giving rise to various unique properties in semiconductor QDs distinct from their unconfined counterpart. The relative scarcity of the studies on the effects of quantum confinement in this system is partially due to the lack of robust synthesis methods for CsPbX₃ QDs with sufficient control of quantum confinement and ensemble uniformity in the strongly confined regime.

Recently, the synthesis of strongly confined CsPbX, QDs with high ensemble uniformity of the size and morphology was achieved, removing one of the obstacles in the exploration of the properties of CsPbX, QDs experiencing strong quantum confinement. The access to the uniform and strongly confined CsPbX, QDs enabled us to disclose a strong and spectrally well-defined induced absorption located between the two lowest allowed exciton transitions in the transient absorption spectra, not discernible in the bulk or weakly-confined system. We attribute this phenomenon to the activation of the forbidden exciton transition by symmetry-breaking polarons formed from the initially excited exciton as illustrated in Figure 1. Its amplitude is nearly half of the exciton bleach amplitude and the bandwidth is comparable to that of bandedge exciton absorption. Weak absorption from formally forbidden transitions due to defects or injected

charge that creates symmetry-breaking perturbation has been reported in a few semiconductor QD systems, *e.g.* CdSe and PbS.¹⁶⁻¹⁹ However, strong activation of the forbidden transition by the photoexcitation of charge-neutral exciton has not been observed previously. The observation in CsPbBr₃ QDs can be explained by the polarons recently reported to form in a spatially non-coincident manner in CsPbBr₃, which may exert a strong symmetry-breaking perturbation on excitons confined in the same space where the polarons form.^{30,21} This observation demonstrates the strong interaction between charge carriers and the lattice, and the importance of this interaction on the optical properties of strongly confined perovskite QDs. Here, we performed a detailed pump-probe transient absorption study in conjunction with electronic structure calculation to gain an understanding on the photoactivation of the forbidden exciton transition in CsPbBr₃ QDs and the possible role of the confined polaron in this process.

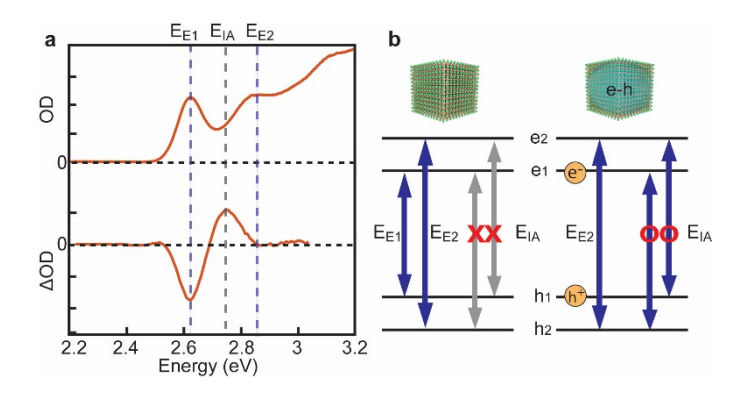


Figure 1. Illustration of the mechanism of light-induced activation of forbidden transition. (a) Static absorption spectrum (top) and transient absorption spectrum at 10 ps time delay (bottom) from CsPbBr₃ QDs with the size of 4.1 nm. The energies of the first and second exciton transitions (E_{E1} , E_{E2}) and the induce absorption (EIA) are indicated with vertical dashed lines. (b) Illustration of the activation of forbidden transition in the presence of photoexcited exciton. e_1 , e_2 , h_1 and h_2 are confined electron and hole levels of CsPbBr₃ QDs.

Results/Discussion

Figure 2a shows a series of optical absorption spectra of strongly confined CsPbBr₃ quantum dots (sample I-V, 3.7-6.9 nm in size) and the larger nanocrystal (sample VI, ~10 nm) experiencing very weak confinement. Comparison of the absorption and photoluminescence for all the samples can be found in Figure S1. Samples I-V were prepared by employing the recently developed method for synthesizing highly uniform CsPbX₃ QDs in the quantum-confined regime, where the thermodynamic equilibrium was utilized as the mechanism to control the size. 15 Sample VI with the average size of ~10 nm was synthesized using the previously reported hot injection methods. 11 The details of the synthesis method and structural characterization of the QDs are presented elsewhere and described briefly in the Methods section. ¹⁵ The representative TEM images of CsPbBr₃ QD samples I, III and V are shown in Figure 2b-d. The absorption spectra of the CsPbBr₃ QDs in Figure 2a exhibit well-resolved bandedge exciton absorption peaks that blueshift with the decreasing size due to the quantum confinement. Additional peaks from the higher-energy transitions are also visible in the absorption spectra. The peaks for the first two excitonic transitions (E_{E1}, E_{E2}) are indicated above each spectrum and their energies are listed in Table 1. The assignment of the peak at E_{E2} to the second exciton transition was confirmed from the bleach appearing at E_{E2} in the transient absorption spectra at high pump intensities saturating the transition at E_{E1} (Figure S2). Table 1 also includes the peak energy of the induced absorption (E_{IA}) in the transient absorption spectra, which is attributed to the forbidden exciton transition in this study.

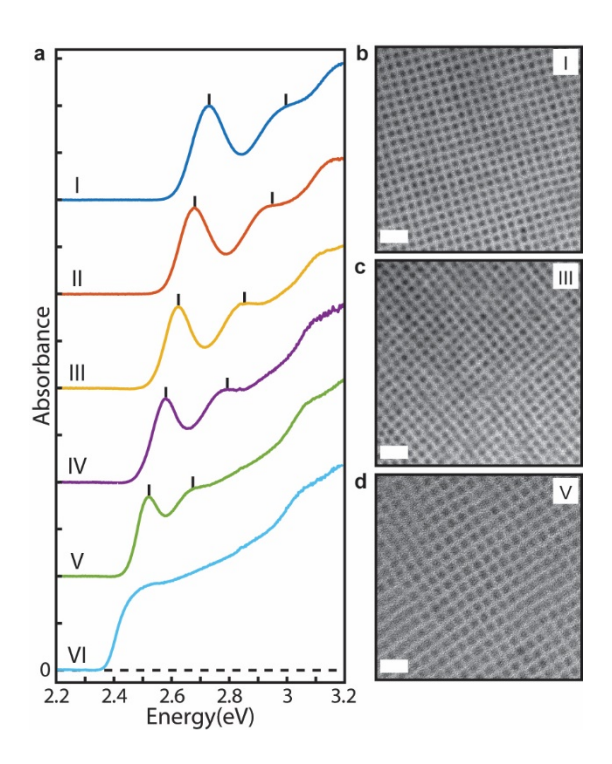


Figure 2. Absorption spectra and TEM images of CsPbBr₃ QDs. (a) Absorption spectra of different sized CsPbBr₃ QDs. Sample VI is the large nanocrystal (~10 nm) with negligible confinement. The peak positions for the two lowest transitions, E_{EI} and E_{EZ}, are indicated above each spectrum. (b)-(d) Representative TEM images of CsPbBr₃ QD samples I, III, and V with the size of 3.7 nm, 4.1 nm and 6.9 nm respectively. Scale bars are 20 nm.

Energy (eV)	I	II	III	IV	V	VI
E _{E1}	2.73	2.68	2.62	2.57	2.51	2.43
E _{E2}	3.00	2.95	2.86	2.79	2.67	-
E _{IA}	2.88	2.83	2.76	2.71	2.60	-

Table 1. Peak energy of the first two exciton transitions ($E_{\scriptscriptstyle EI}$ and $E_{\scriptscriptstyle EZ}$) in the absorption spectra of Figure 1, and the peak energy of the induced absorption ($E_{\scriptscriptstyle IA}$) in the transient absorption spectra in Figure 2f-i. $E_{\scriptscriptstyle EZ}$ in sample VI is unresolvable.

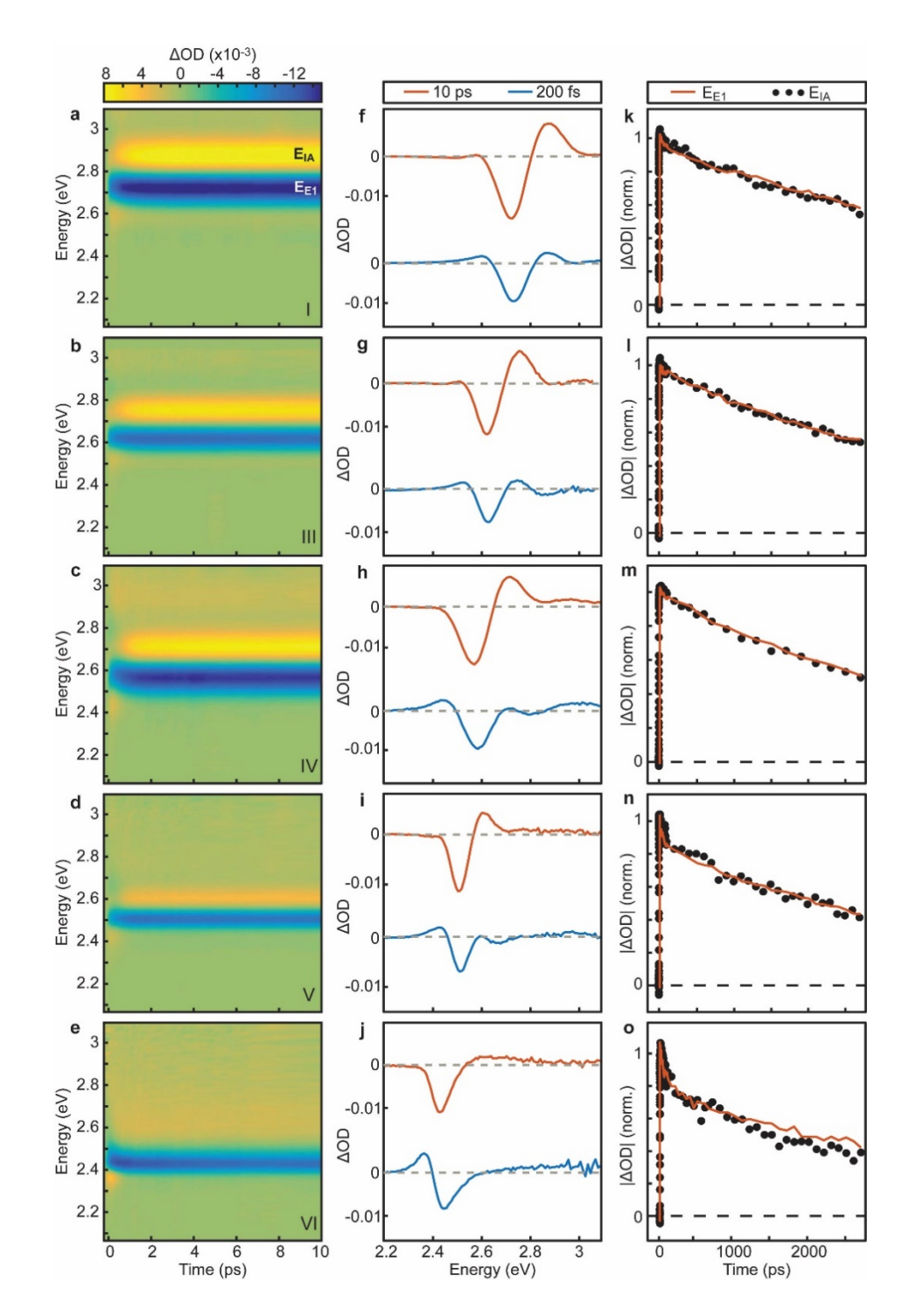


Figure 3. Transient absorption spectra of CsPbBr₃ QDs. (a)-(e) Transient absorption spectra of CsPbBr₃ samples (I, III, IV, V, VI) obtained with 395 nm (3.14 eV) pump for the first 10 ps. (f)-(j) Transient absorption spectra at 200 fs (blue) and 10 ps (red) delay time. (k)-(o) Normalized dynamics of the bleach at E_{EI} (red) and the induced absorption at E_{IA} (black dot). For sample VI, E_{IA} was taken at the peak of the broad induced absorption.

Figure 3a-e compares the dynamic transient absorption spectra of CsPbBr, QDs (sample I, III, IV, V) and weakly confined nanocrystal (sample VI), which show the intense induced absorption attributed to the formally forbidden transition in strongly confined QDs. Two prominent features are observed in the transient absorption spectra of all confined CsPbBr₃ QDs (Figure 3a-d), i.e., the bleach of the bandedge exciton absorption at E_{E} (dark blue feature) and the induced absorption at $E_{\text{\tiny LA}}$ (bright yellow feature) located in between $E_{\text{\tiny EI}}$ and $E_{\text{\tiny EZ}}$. Such spectral features are more clearly seen in Figure 3f-i, where the transient absorption spectra at 10 ps time delay (red) are shown. In contrast, the induced absorption is weaker and spectrally much less distinct in sample VI (Figure 3e and j), likely due to the combination of the congestion of the transitions and the weaker perturbation responsible for activating the forbidden transition in the weakly confined system. This may be a reason why the light-induced activation of the forbidden transition could not be easily revealed in the earlier studies on bulk and weakly confined nanocrystals of CsPbBr₃. The energy of the induced absorption (E_{1A}) in Table 1 was obtained from the fitting of the transient absorption spectra. It is higher than E_{EI} by 100-150 meV depending the QD size and is positioned close to the midpoint of E_{E1} and E_{E2} , which is consistent with the calculated energy of the lowest-energy parity forbidden transition as will be discussed shortly.

Another spectral feature observed in all the samples is the short-lived (<1ps) induced absorption on the lower-energy side of the bandedge exciton bleach. To more clearly show this feature, the transient absorption spectra at 200 fs time delay (blue) are shown in Figure 3f-j. This short-lived induced absorption has also been observed in weakly or non-confined CsPbBr₃. ²¹⁻²³ A similar feature was observed in other semiconductor QDs as well, such as CdSe, and has been explained as the time-varying spectral shift of the bandedge exciton absorption in the presence of pump-excited exciton, *i.e.*, absorption of probe light into biexciton state. ²⁴⁻²⁵ In this 'biexciton'

picture, the rapid sub-ps decay dynamics of the signal reflects the cooling of the initially excited exciton to the bandedge state.²⁴ Although the same interpretation has been made for CsPbBr₃ nanocrystals in some literature due to the seeming similarity to II-VI QDs, other studies have presented evidence that the sub-ps dynamics reflects the polaron formation.^{21,23,26} Our study indicates that the sub-ps decay dynamics of the short-lived induced absorption below the bandgap is more consistent with 'polaron' picture as will be discussed in detail later.

Figure 3k-o compares the normalized dynamics of the bleach recovery at $E_{\scriptscriptstyle \rm El}$ and decay of the induced absorption at E_{IA} on ns time scale, which are essentially identical in all CsPbBr₃ QDs. This indicates the close connection between the optical transition giving rise to the induced absorption and the exciton created by the pump pulse. However, it is not sufficient to unravel the mechanism of the appearance of the induced absorption and the role of exciton in this process. More conclusive evidence for the light-induced activation of the forbidden transition as its origin is obtained from the comparison of the early-time dynamics on ps time scale for all three major spectral features in conjunction with the calculation of the confined electron and hole level structure in CsPbBr₃ QDs. Figure 4 compares the normalized dynamics of the bleach at E_{E1}, induced absorption at E1A, and short-lived induced absorption for a few chosen CsPbBr3 QDs (sample I, III, IV) during the first 5 ps. The average time constants for the rise and decay of the bleach at $E_{\text{\tiny EI}}(\tau_{\text{\tiny EI}})$, induced absorption at $E_{\text{\tiny IA}}(\tau_{\text{\tiny IA}})$ and short-lived induced absorption $(\tau_{\text{\tiny SI}})$ for each sample are listed in Table 2. In the following, we will first discuss the absorption from the formally forbidden transition as the origin of the strong induced absorption at E_{IA}. Next, the lightinduced activation of the forbidden transition and the involvement of polaron in this process will be discussed.

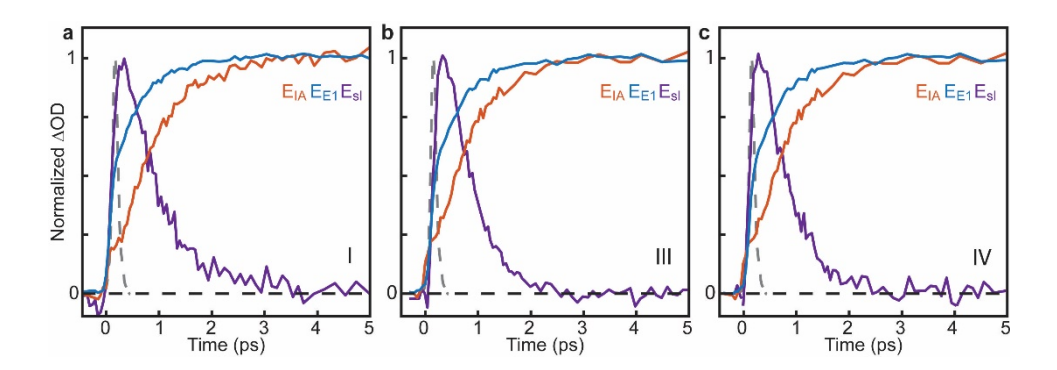


Figure 4. Normalized early-time dynamics of the bleach at $E_{\text{\tiny EI}}$ (blue), induced absorption at $E_{\text{\tiny IA}}$ (red) and the short-lived induced absorption at $E_{\text{\tiny SI}}$ (purple) for a few chosen samples. (a) sample I. (b) sample III. (c) sample IV. $E_{\text{\tiny SI}}$ is chosen where the amplitude of the induced absorption is the largest. Grey dashed curves are pump-probe cross-correlation with fwhm of ~80 fs.

τ (ps)	I	III	IV
$ au_{ ext{EI,decay}}$	5500 ± 150	4400 ± 250	4000 ± 200
$ au_{ ext{El}, ext{rise}}$	0.55 ± 0.03	0.49 ± 0.03	0.44 ± 0.02
$ au_{ ext{IA,decay}}$	5500 ± 250	4400 ± 150	4000 ± 200
$ au_{ ext{IA}, ext{rise}}$	0.85 ± 0.02	0.7 ± 0.05	0.66 ± 0.03
$ au_{ m sl,decay}$	0.83 ± 0.01	0.65 ± 0.02	0.68 ± 0.01

Table 2. Time constants (τ) for the rise and decay of the bleach(τ_{EI}), induced absorption (τ_{IA}), and short-lived induced absorption (τ_{AI}) for sample I, III and IV. The short-lived induced absorption shows the instrument-limited rise (80 fs).

In typical semiconductor QDs, the induced absorption exhibiting the same decay dynamics as the bleach recovery can come from several different processes. One is the intraband absorption of the charge carriers created by the pump pulse. However, the intraband transition occurs at much lower energy than the exciton transition, typically in near to mid infrared region, therefore does not account for the induced absorption appearing in 2.5-3 eV range. 21.29 Transition involving the transfer of the photoexcited charge carriers across the QD interface, e.g., charge transfer to ligand, is also unlikely, considering the high transition energy of >2.5 eV. Another source of induced absorption in the semiconductor QDs that can appear near the bandedge exciton absorption is the biexcitonic absorption. ^{24,25} In the presence of exciton created by the pump pulse, the absorption of the probe light preparing a biexciton state can be spectrally shifted with respect to the ground state exciton absorption, resulting in an induced absorption near the bleach. In the case of extensively studied CdSe QDs, the most distinct biexcitonic feature comes from the lowest-energy biexciton state ($|1s_h-1s_e|$, $|1s_h-1s_e|$).²⁵ It appears at the lower-energy side of the bandedge exciton bleach and it decays on the time scale of hot carrier cooling. In principle, the higher-energy biexciton can give rise to the induced absorption above the bandedge exciton energy, which was previously proposed to explain the broad induced absorption observed in large CsPbBr₃ nanocrystals under very weak confinement.^{22,30} However, it is unlikely that the induced absorption at E₁ in CsPbBr₃ QDs has its origin in biexciton for several reasons. Firstly, the induced absorption from the higher-energy biexciton should be accompanied by a bleach of the higher-energy exciton absorption (e.g., at E_{E}) resulting from the spectral shift in the transient absorption spectrum. The absence of the bleach at the higher-energy exciton transition despite the appearance of the prominent induced absorption at E_{IA} is inconsistent with the biexciton picture. Secondly, the rise time of the induced absorption $(\tau_{\text{\tiny lArise}})$ in Table 2 is quite different from

the rise time of the exciton bleach ($\tau_{\text{\tiny EI,rise}}$) that reflects hot carrier cooling. The disparity of these time scales rules out the biexciton scenario as the origin of the induced absorption at $E_{\text{\tiny EI}}$. We will shortly show the evidence supporting that $\tau_{\text{\tiny EA,rise}}$ is in fact in accordance with the time scale of the polaron formation rather than hot carrier cooling.

The induced absorption at E_{IA} in CsPbBr₃ QDs can be explained by the absorption from the formally forbidden transition activated by the initially excited exciton, which sustains during the whole lifetime of exciton as observed in Figure 3k-o. In principle, the forbidden transitions in QDs can be activated if the exciton or charge carriers excited by the pump creates sufficiently strong perturbation to modify the selection rule for the exciton transition. In fact, possible activation of the forbidden transition from the photoexcitation of exciton has been discussed in several Pb chalcogenide QDs in earlier studies. In PbSe QDs, a weak induced absorption above the bandgap in the transient absorption spectrum was attributed to the forbidden transition turned on by exciton, although the lack of full spectral dynamics makes the assignment less conclusive.31 A different observation was made in a more recent study on PbS QDs, where only hot carriers with sufficiently large excess energy were observed to impart the oscillator strength to the forbidden transitions, in contrast to the case of PbSe QDs.18 The authors augured that a symmetry-breaking transient dipole turning on the forbidden transition is created only by the bulk-like hot carriers not by the bandedge exciton, whose effect persists only during the period of hot carrier cooling on sub-ps time scale.

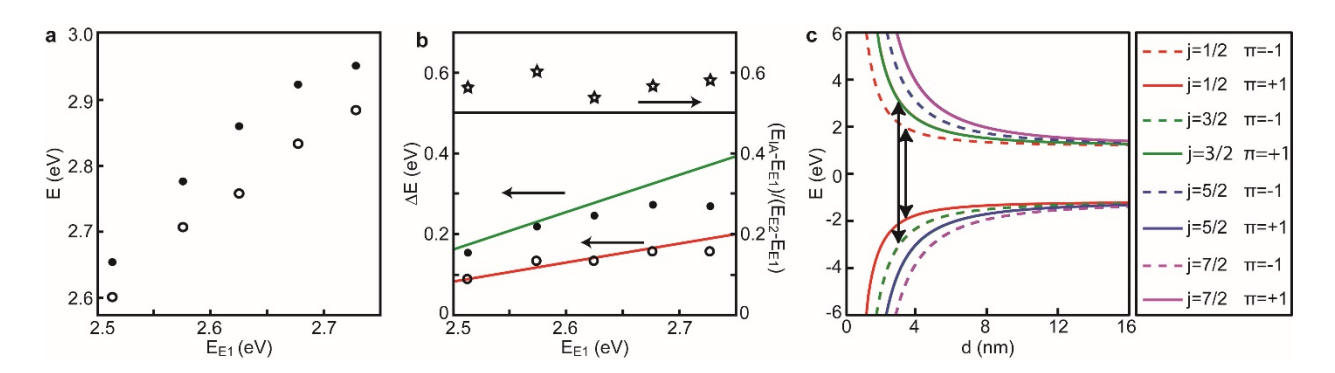


Figure 5. Experimental and calculated exciton transition energies in CsPbBr₃ QDs of different sizes. (a) E_{IA} (open circle) and E_{E2} (closed circle) vs E_{E1} . (b) E_{IA} - E_{E1} (open circle), E_{E2} - E_{E1} (closed circle), and their ratio (star) E_{IA} - E_{E1} / E_{E2} - E_{E1} vs E_{E1} for CsPbBr₃ QDs of different sizes. (c) Size-dependent electron and hole levels of model CsPbBr₃ QDs with different total angular momentum (j) and parity (π) calculated using envelope function approach. d is the diameter of the QD.

For CsPbBr, QDs exhibiting spectrally well-defined and relatively narrow induced absorption peak, the origin of the induced absorption can be more conclusively assigned to the formally forbidden exciton transition activated by the photoexcitation of exciton. An important clue on the nature of the transition giving rise to the induced absorption is found from the comparison of the experimentally measured E_{EL} E_{EL} and E_{EL} with those obtained from the electronic structure calculation. In Figure 5a, E_{EL} and E_{EL} of different-sized CsPbBr, QDs are plotted vs E_{EL} that blueshifts with decreasing QD size due to the quantum confinement. The gap between the two transition energies shown in Figure 5b also widens with increasing E_{EL} (decreasing size) for both E_{EL} - E_{EL} and E_{EL} - E_{EL} as expected from the quantum-confined interband transitions. Furthermore, the ratio of the two quantities, $(E_{EL}$ - $E_{EL})/(E_{EL}$ - E_{EL}), is nearly size-independent, consistent with all three transitions under the same quantum confinement. All the features of the data plotted in Figure 5b are reproduced quite well with the quantum-confined electron and hole energy levels of CsPbBr,

QDs calculated employing the envelope function approach. The details of the calculation and model employed are included in Supplementary Information. The calculated size-dependent energy levels of the confined electron and hole states with different total angular momentum (j) and parity (π) are plotted in Figure 5c. The first two allowed transitions are indicated as the arrows in Figure 5c, which pair the electron and hole states with different parity. The first forbidden transition pairing the electron and hole states of the same parity is energetically positioned in between the two allowed transitions. Theoretical E_{α} - E_{α} , E_{α} - E_{α} and their ratio obtained from the electronic structure calculation, ignoring the exciton binding energy, are overlaid as the solid lines in Figure 5b. The small mismatch between the experimental and calculated quantities, most likely resulting from the ignored exciton binding energy with increases with E_{α} , which is also consistent with the increase of the exciton binding energy with increasing quantum confinement generally expected in QDs. The above results strongly support the photoinduced activation of the parity-forbidden transition as the origin of the induced absorption at E_{α} .

Further insights into the mechanism of activating the forbidden transition in CsPbBr₃ QDs is obtained from the early-time dynamics of the induced absorption in Figure 4 and recent findings on the formation of polaron in lead halide perovskites. In Table 2, the rise time of the induced absorption (τ_{tarisc}) is significantly longer than both the rise time of the bleach (τ_{tarisc}) and the rise time (instrument limited, ~80 fs) of the short-lived induced absorption. On the other hand, τ_{tarisc} is nearly identical to the decay time of the short-lived induced absorption ($\tau_{talaccs}$) in all CsPbBr₃ QDs, suggesting the same origin for these two dynamic features. This can be explained by polaron that is known to form in many perovskite materials from the initially photoexcited exciton as follows. Recently, Zhu and coworkers reported that polarons in bulk single crystal CsPbBr₃ forms on the

time scale of 0.6-0.7 ps.²¹ They also reported that electron and hole polarons form at spatially different location in the lattice, which may create the symmetry-breaking needed to activate the parity-forbidden transition observed in CsPbBr₃ QDs. In their study, the transient absorption coefficient ($\Delta\alpha$) spectrum exhibited a sub-ps dynamic spectral feature below the bandgap, which resembles the short-lived induced absorption in CsPbBr₃ QDs in our study. They explained it with the dynamic screening of Coulomb interaction by polaron, which results in the spectral shift of the probe absorption on the time scale of polaron formation. The involvement of polaron was further corroborated by the time-resolved Kerr effect measurement sensing the lattice distortion by polaron that exhibited the same sub-ps dynamics as $\Delta\alpha$. This indicates that both $\tau_{\mbox{\tiny slateay}}$ and $\tau_{\mbox{\tiny lA,rise}}$ of CsPbBr₃ QDs reflect the time scale of the same process, i.e. the formation of polaron from the initially excited exciton by the pump pulse. Combined with the fact that the induced absorption at $E_{\text{\tiny IA}}$ exhibit the identical decay dynamics as the bleach recovery (i.e., $\tau_{\text{\tiny IA,decay}} = \tau_{\text{\tiny EI,decay}}$), the above analysis strongly supports the polaron as the main source of perturbation activating the forbidden transition. The possibility of the trapped charges as the source of the symmetry-breaking perturbation is ruled out, since the luminescence quantum yield of the QDs is very high (80-95%) and $\tau_{\text{\tiny Hadecay}}$ is also very close to the photoluminescence lifetime. (Figure S3) The present study provides strong evidence for the involvement of polaron in activating the forbidden exciton transition in strongly confined CsPbBr₃ QDs. However, the microscopic nature of the perturbation created by the polaron is still not clear, requiring further experimental and theoretical investigation.

It is notable that the induced absorption from the forbidden transition in strongly confined CsPbBr₃ QDs is much more prominent than in the larger nanocrystals (Sample IV) with very weak confinement. In bulk, careful inspection of the $\Delta\alpha$ spectrum from Ref. 21 reveals only a

faint signature of broad induced absorption above the bandgap similarly to the larger weakly confined CsPbBr, nanocrystals. The unusually strong absorption from the forbidden transition in strongly confined QDs may reflect the fact that the polaron occupies the same confined space as the exciton excited by the probe light, imposing the stronger perturbation on exciton transition. An interesting question that arises from the foregoing discussion is whether other forbidden transitions at the higher energy can also be activated. While the limited spectral coverage of the probe light in the UV range in our study limits the ability to probe other higher-energy transitions, a weaker induced absorption above E_{tx} is observed in Figure 3c centered around 3.0 eV. The weaker induced absorption appearing above E_{tx} is more clearly identifiable in the transient absorption spectra at 10 ps shown in Figure 3h. Interestingly, the higher-energy induced absorption also shows the same decay dynamics as the one at E_{tx} as shown in Figure S4. This indicates that more than one forbidden transition can be activated by the photoexcitation of exciton, while the magnitude of activation may vary.

Conclusions

In summary, we have observed the strong photoinduced activation of the forbidden transitions in CsPbBr₃ QDs giving rise to an intense and spectrally well-defined induced absorption in the transient absorption spectra located between the two dipole-allowed excitonic transitions. Unlike in many other semiconductor QDs, photoexcitation of exciton in CsPbBr₃QDs creates a sufficiently large perturbation that can activate the forbidden exciton transition, which sustains during the entire lifetime of exciton. The photoactivation of the forbidden transition in CsPbBr₃ QDs is considered mediated by the symmetry-breaking polarons created after the excitation of exciton in the QDs. The activation of the forbidden transition is particularly

prominent in strongly confined QDs due to the confinement of exciton in the same space polaron forms. The present study demonstrates how the intimate interaction of photoexcited exciton with the lattice in a confined space gives an access to the forbidden transition by breaking the optical selection rule in CsPbBr₃ QDs. The light-induced enhancement of the absorption strength through the opening of the forbidden optical transition channel could be applicable in obtaining more efficient optical pumping in the photonic application using perovskite QDs.

Methods/Experimental

Preparation of CsPbBr, Quantum Dots. A list of chemicals used in the synthesis is found in the Supplementary Information. The Cs-oleate precursor was prepared by dissolving Cs₂CO₃ (2.5 g) in an oleic acid (OA, 0.8 g) and 1-octadecene (ODE, 7 g) mixture at 150 °C under N₂ atmosphere on a Schlenk line. The Pb and Br precursor solutions were prepared by dissolving 75 mg of PbBr₂ and 0-600 of mg ZnBr₂ in the mixture of 5 mL ODE, 2 mL OA, and 2 mL oleylamine (OAm) at 120 °C under N₂ atmosphere. The amount of ZnBr₂ was varied depending on the target QD size. After selecting the temperature for the synthesis of the desired QD size, 0.4 mL of the Cs-oleate precursor was injected into the precursor solution of Pb and Br to initiate the reaction. Since the QD size was controlled via thermodynamic equilibrium, the final size of the QD was determined only by the concentration of the reactant and the temperature independent of the kinetics of the reaction. Once the QDs of the desired sizes are formed, the reactant mixture was cooled in an ice bath to quench the reaction. The QDs were recovered by centrifuging the reaction product at 3500 rpm and redispersed in hexane for all optical measurements. A more detailed description of the synthesis and cleaning procedures can be found in Ref. 15.

Transient Absorption Measurements. Transient absorption (TA) measurements were made using a home-built pump-probe absorption spectrometer. 395 nm pump pulses were generated by doubling 790 nm output (80 fs autocorrelation 3 kHz) from a Ti:sapphire amplifier (KM Labs) in a 300 μ m-thick BBO crystal. The pump beam fluence was attenuated to keep the excitation density in the QD sufficiently low to minimize the effect of exciting multiple excitons, such as Auger relaxation. Under typical experimental condition, the maximum bleach amplitude at the bandedge was ~5 % of the absorption intensity, which was achieved at the fluence of 3.5x10⁴ J/cm² for the case of sample III for instance. A higher pump fluence was used to confirm the appearance of the second bleach at E₁₂ in the transient absorption data, which was assigned to the second exciton transition in the linear absorption spectra. The white-light supercontinuum probe was generated by focusing a couple μJ of 790 nm beam onto a 1 mm-thick CaF₂ window. The transient absorption data were recorded either as the full time-dependent spectrum using a pair of CMOS spectrometers (Ocean Optics STS-VIS) or as a kinetic trace at a chosen probe wavelength using a pair of amplified Si photodiodes and a monochromator (Newport, Oriel Cornerstone 130). The transient absorption spectra recorded in full spectral range of the probe were corrected for the chirp in the supercontinuum before further analysis. In all the measurements, the QD samples dispersed in cyclohexane were continuously circulated in a 2 mm-thick quartz flowing cell to avoid any potential photodegradation of the sample. The typical pump-probe cross correlation measured on a BBO crystal was 80 fs.

Envelope Function Approach for CsPbBr₃ QDs. A four-band envelope function approach is applied to calculate the electronic structure of a CsPbBr₃ quantum dot with spherical boundary

condition. Bulk CsPbBr₃ has a direct band gap located at the Γ point with doubly degenerate Γ_6^+

valence band maximum and Γ_6^- conduction band minimum. We then build the corresponding

 $4 \times 4 \mathbf{k} \cdot \mathbf{p}$ Hamiltonian matrix $\mathbf{H_0}$ at Γ point incorporating materials dependent parameters such

as bandgap, effective electron/hole mass, and spin-orbit coupling strength. The eigenfunctions

are constructed from linear combination of spherical harmonics. Spherical boundary condition is

used, outside which the eigen wavefunctions decay to zero. This leads to a set of six nonlinear

equations that are solved in a self-consistent iterative scheme.³² The effective electron/hole mass

is evaluated from the second order derivatives of band dispersion (Figure S5) at Γ point using

density functional theory (DFT) with the Perdew-Burke-Ernzerhof (PBE) exchange-correlation

functional, spin-orbit coupling, and first-principles tight-binding method.³⁵⁻³⁸ For the envelope

function calculation, the band gap, underestimated by DFT-PBE, is further corrected by the

experimental value of 2.36 eV.

ASSOCIATED CONTENT

Supporting Information. The Supporting Information is available free of charge on the ACS

Publications website at DOI: Absorption and PL spectra from each sample, transient absorption

data at higher pump powers, time dependent PL data, and details of the electronic structure

calculations. The authors declare no competing financial interest.

AUTHOR INFORMATION

Corresponding Author

*Email: <u>dhson@chem.tamu.edu</u>

ORCID: 0000-0001-9002-5188

19

ACKNOWLEDGMENT

This research was supported by the Robert A. Welch Foundation A-1639 (D.R.) and IBS-R026-D1 (D.H.S.). H.W. and X.Q. acknowledge the support by National Science Foundation under award number DMR-1753054. Portions of this research were conducted with the advanced computing resources provided by Texas A&M High Performance Research Computing and support from TAMU-STRP.

REFERENCES

- Swarnkar, A.; Marshall, A. R.; Sanehira, E. M.; Chernomordik, B. D.; Moore, D. T.; Christians, J. A.; Chakrabarti, T.; Luther, J. M. Quantum Dot–Induced Phase Stabilization of α-CsPbI₃ Perovskite for High-Efficiency Photovoltaics. *Science* 2016, 354, 92-95.
- Nedelcu, G.; Protesescu, L.; Yakunin, S.; Bodnarchuk, M. I.; Grotevent, M. J.; Kovalenko, M. V. Fast Anion-Exchange in Highly Luminescent Nanocrystals of Cesium Lead Halide Perovskites (CsPbX₃, X = Cl, Br, I). *Nano Lett.* 2015, 15, 5635-5640.
- 3. Yakunin, S.; Protesescu, L.; Krieg, F.; Bodnarchuk, M. I.; Nedelcu, G.; Humer, M.; De Luca, G.; Fiebig, M.; Heiss, W.; Kovalenko, M. V. Low-Threshold Amplified Spontaneous Emission and Lasing From Colloidal Nanocrystals of Cesium Lead Halide Perovskites. *Nat. Commun.* **2015**, *6*, 8056-8092.
- 4. Stranks, S. D.; Eperon, G. E.; Grancini, G.; Menelaou, C.; Alcocer, M. J. P.; Leijtens, T.; Herz, L. M.; Petrozza, A.; Snaith, H. J. Electron-Hole Diffusion Lengths Exceeding 1

 Micrometer in an Organometal Trihalide Perovskite Absorber. *Science* 2013, 342, 341-344.
- 5. Ramasamy, P.; Lim, D. H.; Kim, B.; Lee, S. H.; Lee, M. S.; Lee, J. S. All-Inorganic Cesium Lead Halide Perovskite Nanocrystals for Photodetector Applications. *Chem. Commun.* **2016**, *52*, 2067-2070.

- Eaton, S. W.; Lai, M.; Gibson, N. A.; Wong, A. B.; Dou, L.; Ma, J.; Wang, L. W.; Leone, S. R.; Yang, P. Lasing in Robust Cesium Lead Halide Perovskite Nanowires. *Proc. Natl. Acad. Sci.* 2016, 113, 1993-1998.
- 7. Beal, R. E.; Slotcavage, D. J.; Leijtens, T.; Bowring, A. R.; Belisle, R. A.; Nguyen, W. H.; Burkhard, G. F.; Hoke, E. T.; McGehee, M. D. Cesium Lead Halide Perovskites With Improved Stability for Tandem Solar Cells. *J. Phys. Chem. Lett.* **2016**, *7*, 746-751.
- 8. Wu, K.; Liang, G.; Shang, Q.; Ren, Y.; Kong, D.; Lian, T. Ultrafast Interfacial Electron and Hole Transfer from CsPbBr₃ Perovskite Quantum Dots. *J. Am. Chem. Soc.* **2015**, *137*, 12792-12795.
- 9. Zhang, X.; Lin, H.; Huang, H.; Reckmeier, C.; Zhang, Y.; Choy, W. C. H.; Rogach, A. L. Enhancing the Brightness of Cesium Lead Halide Perovskite Nanocrystal Based Green Light-Emitting Devices Through the Interface Engineering with Perfluorinated Ionomer. *Nano Lett.* **2016**, *16*, 1415-1420.
- 10. Brennan, M. C.; Herr, J. E.; Nguyen-Beck, T. S.; Zinna, J.; Draguta, S.; Rouvimov, S.; Parkhill, J.; Kuno, M. Origin of the Size-Dependent Stokes Shift in CsPbBr₃ Perovskite Nanocrystals. *J. Am. Chem. Soc.* **2017**, *139*, 12201-12208.
- 11. Protesescu, L.; Yakunin, S.; Bodnarchuk, M. I.; Krieg, F.; Caputo, R.; Hendon, C. H.; Yang, R. X.; Walsh, A.; Kovalenko, M. V. Nanocrystals of Cesium Lead Halide Perovskites (CsPbX₃, X = Cl, Br, and I): Novel Optoelectronic Materials Showing Bright Emission With Wide Color Gamut. *Nano Lett.* **2015**, *15*, 3692-3696.
- 12. Haque, A.; Ravi, V. K.; Shanker, G. S.; Sarkar, I.; Nag, A.; Santra, P. K. Internal Heterostructure of Anion-Exchanged Cesium Lead Halide Nanocubes. *J. Phys. Chem. C* **2018**, *122*, 13399-13406.
- 13. Almeida, G.; Goldoni, L.; Akkerman, Q.; Dang, Z.; Khan, A. H.; Marras, S.; Moreels, I.; Manna, L. Role of Acid–Base Equilibria in the Size, Shape, and Phase Control of Cesium Lead Bromide Nanocrystals. *ACS Nano* **2018**, *12*, 1704-1711.
- 14. Dutta, A.; Dutta, S. K.; Das Adhikari, S.; Pradhan, N. Tuning the Size of CsPbBr₃

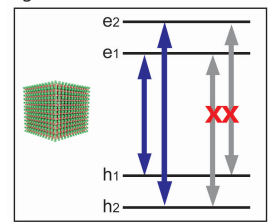
 Nanocrystals: All at One Constant Temperature. *ACS Energ. Lett.* **2018**, *3*, 329-334.
- 15. Dong, Y.; Qiao, T.; Kim, D.; Parobek, D.; Rossi, D.; Son, D. H. Precise Control of Quantum Confinement in Cesium Lead Halide Perovskite Quantum Dots *via* Thermodynamic Equilibrium. *Nano Lett.* **2018**, *18*, 3716-3722.

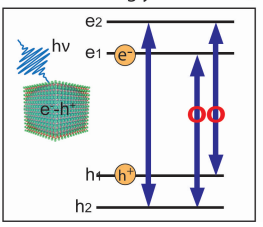
- 16. Nootz, G.; Padilha, L. A.; Olszak, P. D.; Webster, S.; Hagan, D. J.; Van Stryland, E. W.; Levina, L.; Sukhovatkin, V.; Brzozowski, L.; Sargent, E. H. Role of Symmetry Breaking on the Optical Transitions in Lead-Salt Quantum Dots. *Nano Lett.* **2010**, *10*, 3577-3582.
- 17. Schmidt, M. E.; Blanton, S. A.; Hines, M. A.; Guyot-Sionnest, P. Polar CdSe Nanocrystals: Implications for Electronic Structure. *J. Chem. Phys.* **1997**, *106*, 5254-5259.
- 18. Trinh, M. T.; Sfeir, M. Y.; Choi, J. J.; Owen, J. S.; Zhu, X. A Hot Electron–Hole Pair Breaks the Symmetry of a Semiconductor Quantum Dot. *Nano Lett.* **2013**, *13*, 6091-6097.
- 19. Spittel, D.; Poppe, J.; Meerbach, C.; Ziegler, C.; Hickey, S. G.; Eychmüller, A. Absolute Energy Level Positions in CdSe Nanostructures From Potential-Modulated Absorption Spectroscopy (EMAS). *ACS Nano* **2017**, *11*, 12174-12184.
- 20. Miyata, K.; Atallah, T. L.; Zhu, X. Y. Lead Halide Perovskites: Vrystal-Liquid Duality, Phonon Glass Electron Crystals, and Large Polaron Formation. *Sci. Adv.* **2017**, *3*, 1701469-1701479.
- 21. Miyata, K.; Meggiolaro, D.; Trinh, M. T.; Joshi, P. P.; Mosconi, E.; Jones, S. C.; De Angelis, F.; Zhu, X.-Y. Large Polarons in Lead Halide Perovskites. *Sci. Adv.* **2017**, *3*, 1701217-1701226.
- 22. Mondal, N.; Samanta, A. Complete Ultrafast Charge Carrier Dynamics in Photo-Excited All-Inorganic Perovskite Nanocrystals (CsPbX₃). *Nanoscale* **2017**, *9*, 1878-1885.
- 23. Makarov, N. S.; Guo, S.; Isaienko, O.; Liu, W.; Robel, I.; Klimov, V. I. Spectral and Dynamical Properties of Single Excitons, Biexcitons, and Trions in Cesium–Lead-Halide Perovskite Quantum Dots. *Nano Lett.* **2016**, *16*, 2349-2362.
- 24. Klimov, V.; Hunsche, S.; Kurz, H. Biexciton Effects in Femtosecond Nonlinear Transmission of Semiconductor Quantum Dots. *Phys. Rev. B* **1994**, *50*, 8110-8113.
- 25. Sewall, S. L.; Franceschetti, A.; Cooney, R. R.; Zunger, A.; Kambhampati, P. Direct Observation of the Structure of Band-Edge Biexcitons in Colloidal Semiconductor CdSe Quantum Dots. *Phys. Rev. B* 2009, 80, 081310-081313.
- 26. Aneesh, J.; Swarnkar, A.; Kumar Ravi, V.; Sharma, R.; Nag, A.; Adarsh, K. V. Ultrafast Exciton Dynamics in Colloidal CsPbBr₃ Perovskite Nanocrystals: Biexciton Effect and Auger Recombination. *J. Phys. Chem. C* **2017**, *121*, 4734-4739.

- 27. Klimov, V. I.; Schwarz, C. J.; McBranch, D. W.; Leatherdale, C. A.; Bawendi, M. G. Ultrafast Dynamics of Inter- and Intraband Transitions in Semiconductor Nanocrystals: Implications for Quantum-Dot Lasers. *Phys. Rev. B* 1999, 60, 2177-2180.
- 28. Deng, Z.; Guyot-Sionnest, P. Intraband Luminescence From HgSe/CdS Core/Shell Quantum Dots. *ACS Nano* **2016**, *10*, 2121-2127.
- 29. Jeong, K. S.; Guyot-Sionnest, P. Mid-Infrared Photoluminescence of CdS and CdSe Colloidal Quantum Dots. *ACS Nano* **2016**, *10*, 2225-2231.
- 30. Hu, Y. Z.; Koch, S. W.; Lindberg, M.; Peyghambarian, N.; Pollock, E. L.; Abraham, F. F. Biexcitons in Semiconductor Quantum Dots. *Phys. Rev. Lett.* **1990**, *64*, 1805-1807.
- 31. Schins, J. M.; Trinh, M. T.; Houtepen, A. J.; Siebbeles, L. D. A. Probing Formally Forbidden Optical Transitions in PbSe Nanocrystals by Time- and Energy-Resolved Transient Absorption Spectroscopy. *Phys. Rev. B* **2009**, *80*, 035323-035328.
- 32. Kang, I.; Wise, F. W. Electronic Structure and Optical Properties of PbS and PbSe Quantum Dots. *J. Opt. Soc. Am. B* **1997**, *14*, 1632-1646.
- 33. Becker, M. A.; Vaxenburg, R.; Nedelcu, G.; Sercel, P. C.; Shabaev, A.; Mehl, M. J.; Michopoulos, J. G.; Lambrakos, S. G.; Bernstein, N.; Lyons, J. L.; Stöferle, T.; Mahrt, R. F.; Kovalenko, M. V.; Norris, D. J.; Rainò, G.; Efros, A. L. Bright Triplet Excitons in Cesium Lead Halide Perovskites. *Nature* **2018**, *553*, 189.
- 34. Elward, J. M.; Chakraborty, A. Effect of Dot Size on Exciton Binding Energy and Electron–Hole Recombination Probability in CdSe Quantum Dots. *J. Chem. Theory Comput.* **2013**, *9*, 4351-4359.
- 35. Hohenberg, P.; Kohn, W. Inhomogeneous Electron Gas. *Phys. Rev. B* **1964**, *136*, B864-B871.
- 36. Kohn, W.; Sham, L. J. Self-Consistent Equations Including Exchange and Correlation Effects. *Phys Rev* **1965**, *140*, A1133-A1138.
- 37. Perdew, J. P.; Burke, K.; Ernzerhof, M. Generalized Gradient Approximation Made Simple. *Phys. Rev. Lett.* **1996**, *77*, 3865-3868.
- 38. Qian, X.; Li, J.; Qi, L.; Wang, C. Z.; Chan, T. L.; Yao, Y. X.; Ho, K. M.; Yip, S. Quasiatomic Orbitals for *ab initio* Tight-Binding Analysis. *Phys. Rev. B* **2008**, *78*, 245112.

TOC

Light-activation of forbidden transition in strongly-confined QD





Supporting Information

Light-Induced Activation of Forbidden Exciton Transition in Strongly Confined Perovskite Quantum Dots

Daniel Rossi^{*}, Hua Wang^{*}, Yitong Dong^{*}, Tian Qiao^{*}, Xiaofeng Qian^{*} and Dong Hee Son^{*}

Department of Chemistry, Texas A&M University, College Station, Texas 77843, United States

Department of Materials Science and Engineering, Texas A&M University, College Station,

Texas 77843, United States

[§]Center for Nanomedicine, Institute for Basic Science (IBS), Seoul 03722, Republic of Korea

Correspondence to: dhson@chem.tamu.edu

Materials used for synthesis

Cesium carbonate (Cs₂CO₃, puratronic, 99.994%, metals basis, Alfa Aesar), Lead (II) bromide (PbBr₂, puratronic, 99.999% metals basis, Alfa Aesar), Zinc bromide (ZnBr₂, 99.9%, metals basis, Alfa Aesar), Oleylamine (OAm, technical grade 70%, Aldrich), Oleic acid (OA, technical grade 90%, Aldrich), 1-Octadecene (ODE, technical grade 90%, Aldrich), Trioctylphosphine (TOP, 97%, Aldrich), Acetone (Certified ACS, Fischer), Hexane (HPLC grade, Millipore), Cyclohexane (HPLC grade, BDH). The detailed synthesis procedure is found in Ref. S1.¹

TEM Measurements

TEM images of CsPbBr₃ quantum dots (QDs) were obtained on a FEI Tecnai G2 F20 ST field-emission TEM microscope at 200 kV.

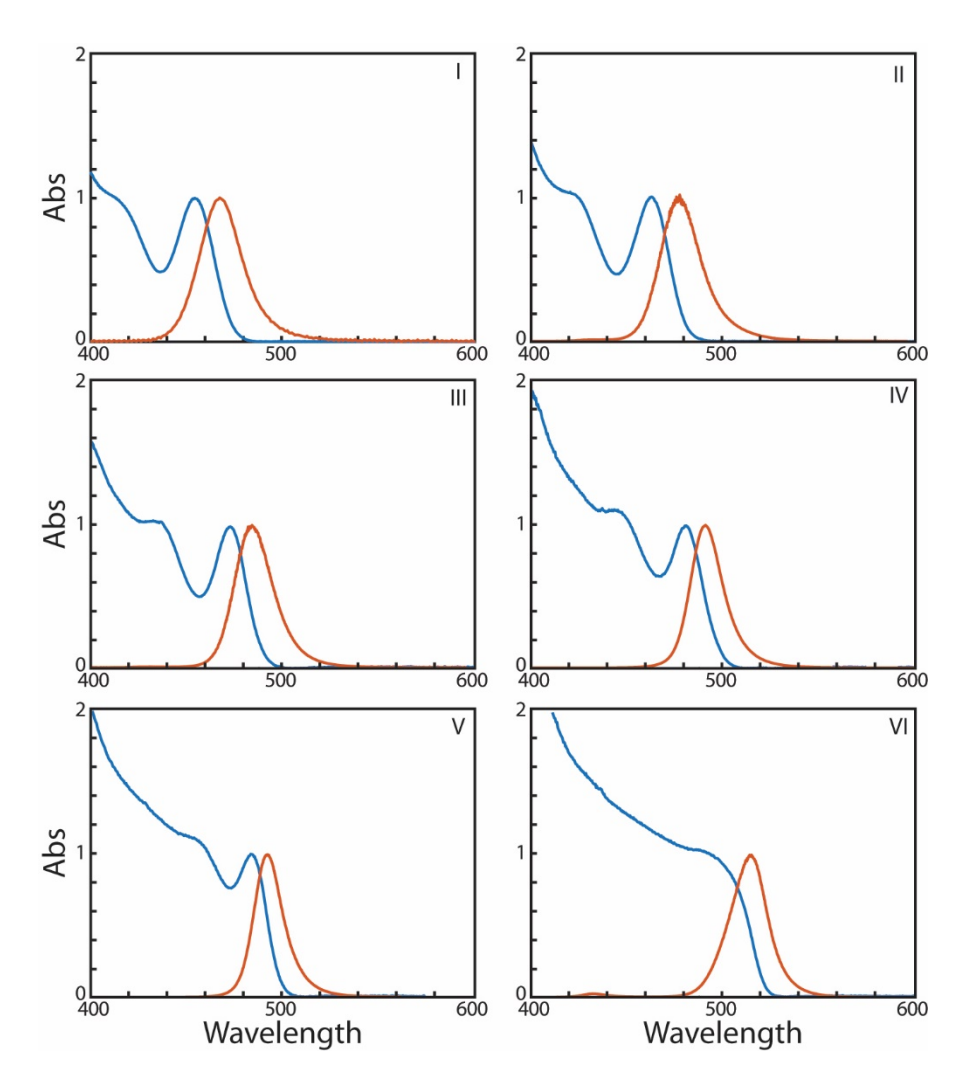


Figure S1. Comparison of absorption and PL spectra for the six samples studied in this experiment.

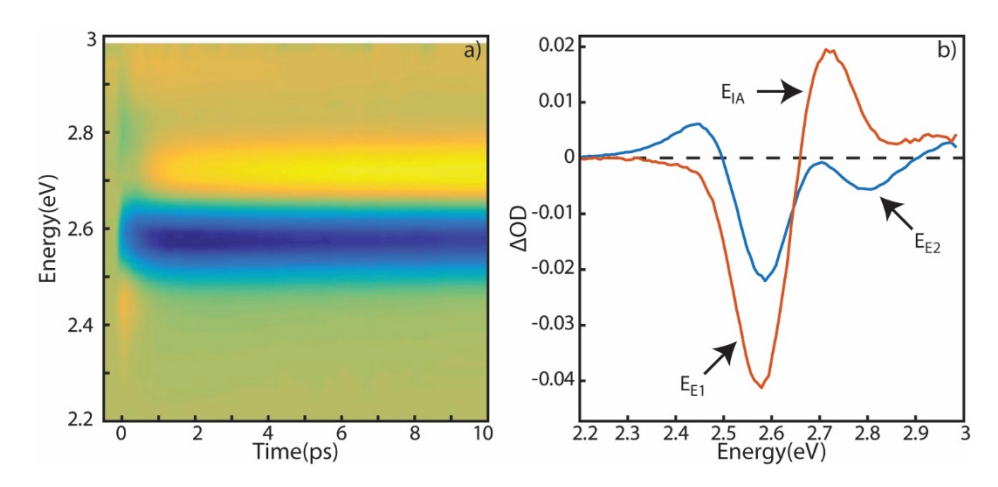


Figure S2. (a) Contour plot of transient absorption spectra of CsPbBr₃ QD sample IV under higher power excitation conditions for the first 10 ps. Bleach of second exciton transition is observed near 2.8 eV at <1ps. (b) Transient absorption spectra at 200 fs (blue) and 10 ps (red) taken from the data in panel a. The second bleach in 200 fs transient absorption spectrum occurs at E_{E2} , which is the same as the second absorption peak identified in the linear absorption spectrum.

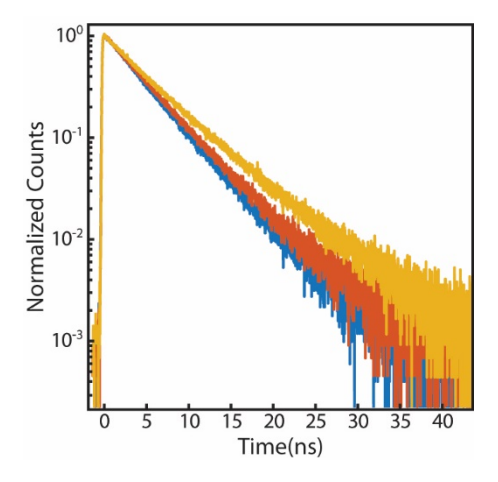


Figure S3. Time-resolved PL data of from CsPbBr₃ QD samples II (blue), III (yellow), and IV (red) obtained from time-correlated single photon counting measurement.

τ (ns)	II	III	IV
$ au_{\mathrm{E}1}$	5.3	4.4	4
T_{PL}	5.4	4.8	4.3

Table S1. Comparison of bandedge PL lifetime and bleach recovery time at E_{E1} decay for $CsPbBr_3\ QD\ sample\ IV\ II,\ III,\ and\ IV.$

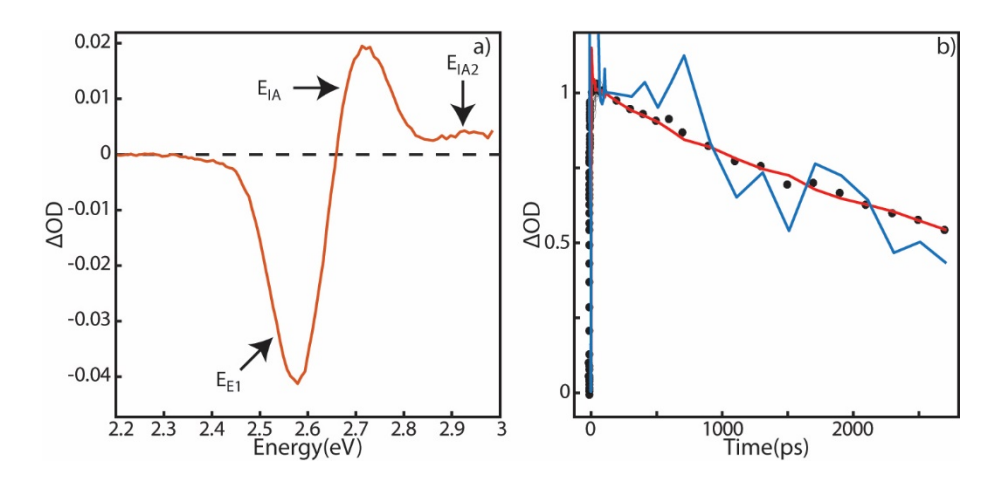


Figure S4. (a) Transient absorption spectrum of CsPbBr₃ QD sample IV at 10 ps delay time under higher power excitation conditions. (b) Comparison of the normalized decay dynamics of the bleach at E_{E1} (red), induced absorption at E_{IA} (black dots) and the higher-energy induced absorption at E_{IA2} (blue).

Electronic Structure Calculations

(1) Envelope function approach for CsPbBr3 quantum dot: Theory

We used a four-band envelope function approach to calculate the electronic structure of a CsPbBr₃ quantum dot with spherical boundary conditions, outside which the eigen wavefunctions decay to zero. Bulk CsPbBr₃ has a direct band gap located at the Γ point. Both the Γ_6^+ valence band maximum and Γ_6^- conduction band minimum are doubly degenerate. The corresponding $4 \times 4 \mathbf{k} \cdot \mathbf{p}$ Hamiltonian matrix $\mathbf{H_0}$ at Γ point is given by²⁻³

$$\mathbf{H_0}(\mathbf{k}) = \begin{bmatrix} \left(\frac{E_g}{2} + \frac{\hbar^2 k^2}{2m_c}\right) \mathbf{I} & \frac{\hbar P}{m_0} \mathbf{k} \cdot \mathbf{\sigma} \\ \frac{\hbar P}{m_0} \mathbf{k} \cdot \mathbf{\sigma} & -\left(\frac{E_g}{2} + \frac{\hbar^2 k^2}{2m_v}\right) \mathbf{I} \end{bmatrix}.$$

Here σ is the Pauli matrix, \mathbf{I} is 2×2 identity matrix, m_0 is the free electron rest mass, and E_g is the bulk band gap. m_c , m_v , and P are materials dependent parameters related to averaged effective mass of conduction and valence bands, and spin-orbit coupling strength which can be fitted from first-principles calculations. The boundary condition of the envelope function $\mathcal{F}(r)$ in the Schrödinger equation $\mathbf{H}_0\mathcal{F}(\mathbf{r}) = E\mathcal{F}(\mathbf{r})$ reads

$$\mathcal{F}(|\mathbf{r}| = a) = 0.$$

a is the radius of the CsPbBr₃ quantum dot. The eigenfunctions can be constructed from linear combination of spherical harmonics. Finally, one can obtain a set of six nonlinear equations that can be solved in a self-consistent iterative scheme³

$$E_{\pm}(k) = \frac{1}{2} \left[\left(\frac{1}{m_{\rm c}} - \frac{1}{m_{\rm v}} \right) \frac{\hbar^2 k^2}{2} \pm \sqrt{\left[\left(E_g + \left(\frac{1}{m_{\rm c}} + \frac{1}{m_{\rm v}} \right) \frac{\hbar^2 k^2}{2} \right)^2 + \left(\frac{2\hbar P}{m_0} \right)^2 k^2 \right]} \right],$$

$$\lambda_{\pm}(k) = \sqrt{\frac{\left(\frac{1}{m_{\rm c}} + \frac{1}{m_{\rm v}}\right)\hbar^2 E_g + \left(\frac{2\hbar P}{m_0}\right)^2 + 2\left(\frac{1}{m_{\rm c}} - \frac{1}{m_{\rm v}}\right)\hbar^2 E_{\pm}(k)}{\left(\left(\frac{1}{m_{\rm c}} + \frac{1}{m_{\rm v}}\right)\frac{\hbar^2}{2}\right)^2 - \left(\left(\frac{1}{m_{\rm c}} - \frac{1}{m_{\rm v}}\right)\frac{\hbar^2}{2}\right)^2} + k^2,$$

$$\begin{cases} \rho_{\pm}(k)J_{l+1}(ka)I_{l}(\lambda_{\pm}(k)a) - \mu_{\pm}(k)J_{l}(ka)I_{l+1}(\lambda_{\pm}(k)a) = 0, & j = l + \frac{1}{2}, \pi = (-1)^{l+1} \\ \rho_{\pm}(k)J_{l}(ka)I_{l+1}(\lambda_{\pm}(k)a) + \mu_{\pm}(k)J_{l+1}(ka)I_{l}(\lambda_{\pm}(k)a) = 0, & j = (l+1) - \frac{1}{2}, \pi = (-1)^{l} \end{cases}$$

$$\begin{cases} \rho_{\pm}(k) = \frac{E_g + \frac{\hbar^2 k^2}{m_c} - 2E_{\pm}(k)}{\frac{2\hbar P}{m_0} k} \\ \mu_{\pm}(k) = \frac{E_g + \frac{\hbar^2 \lambda_{\pm}^2(k)}{m_c} - 2E_{\pm}(k)}{\frac{2\hbar P}{m_0} \lambda_{\pm}(k)} \end{cases}$$

Here, \pm indicate conduction (+) and valence (-) energy levels. J_l and I_l are the first kind spherical and modified spherical Bessel functions. λ_{\pm} , ρ_{\pm} , and μ_{\pm} have the same unit as k, 1/k and 1/k, respectively. π indicates the parity of the wavefunction. j and l are total and azimuthal quantum numbers, respectively.

(2) Envelope function approach for CsPbBr3 quantum dot: Results

Figure S5 shows the electronic band structure of bulk CsPbBr₃ calculated by density functional theory (DFT)⁴⁻⁵ with the Perdew-Burke-Ernzerhof (PBE) exchange-correlation functional,⁶ spin-orbit coupling, and first-principles tight-binding method.⁷ The effective mass is evaluated by second order derivatives of band dispersion at Γ point, subsequently averaged along x, y, and z directions. In addition, the band gap, underestimated by DFT-PBE, is corrected by the experimental value of 2.36 eV in the envelope function calculation. The corresponding parameters are listed in Table S2.

Figure 4c shows the final electronic levels in CsPbBr₃ quantum dot with varying particle diameter (d). The allowed and forbidden optical transitions are subsequently calculated using these electronic levels with corresponding selection rules.

	$E_{\rm g}\left({ m eV}\right)$	$m_{\rm c} (m_0)$	$m_v(m_0)$	$P^2 (eV*m_0)$
CsPbBr ₃	2.36	0.1826	0.1750	6.6

Table S2. Parameters used in the envelope function approach for determining electronic levels in CsPbBr₃ quantum dot with varying radius.

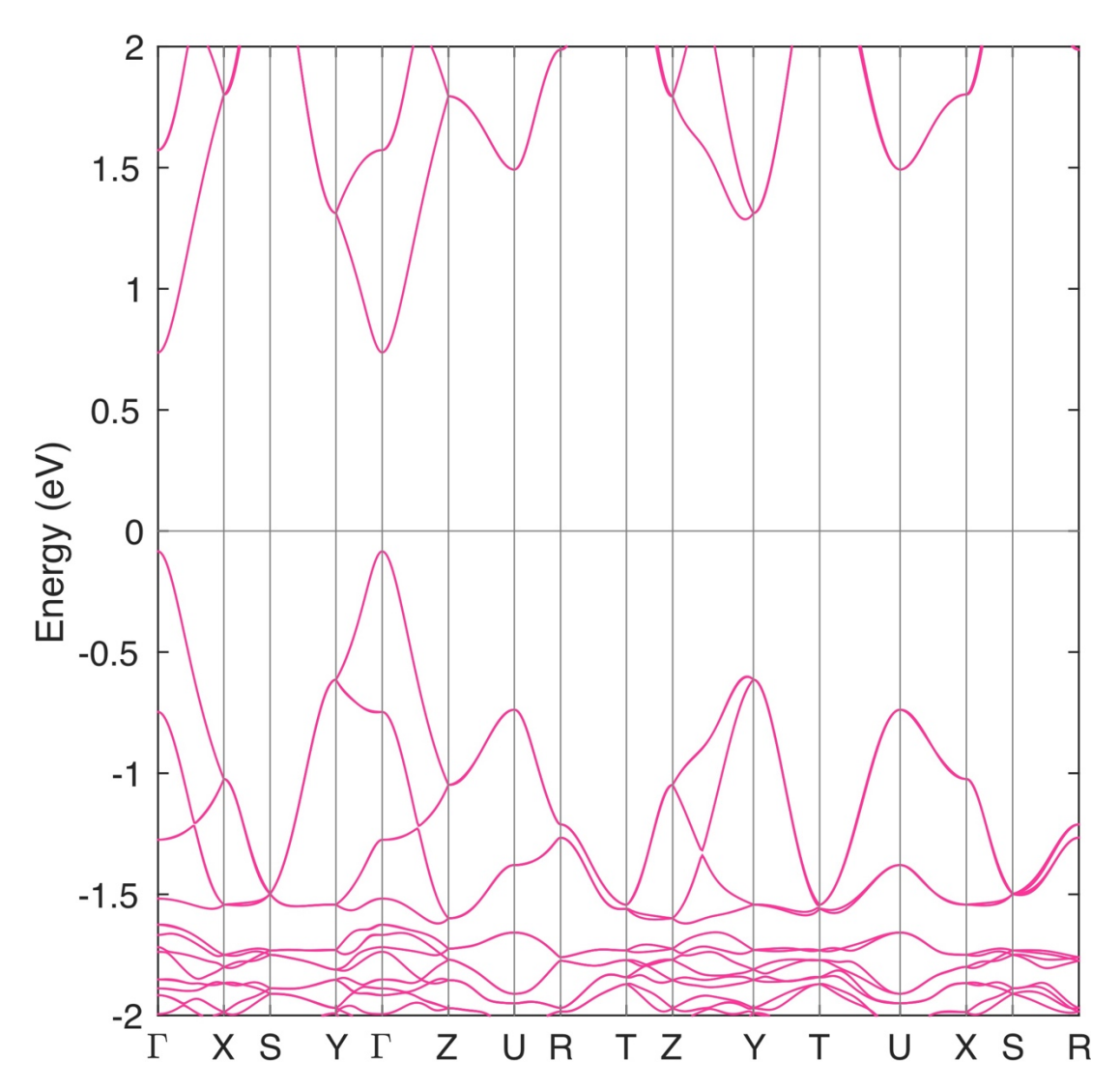


Figure S5. Electronic band structure of bulk CsPbBr₃, calculated by density functional theory (DFT) with the Perdew-Burke-Ernzerhof (PBE) exchange-correlation functional and spin-orbit coupling. The effective mass is evaluated by the second order derivatives of band dispersion at Γ point, subsequently averaged along x, y, and z directions. In addition, in the envelope function calculation the band gap underestimated by DFT-PBE is further corrected according to the experimental value of 2.36 eV.

References

- S1. Dong, Y.; Qiao, T.; Kim, D.; Parobek, D.; Rossi, D., et al., Precise Control of Quantum Confinement in Cesium Lead Halide Perovskite Quantum Dots via Thermodynamic Equilibrium. *Nano Lett.* **2018**, *18*, 3716-3722.
- S2. Becker, M. A.; Vaxenburg, R.; Nedelcu, G.; Sercel, P. C.; Shabaev, A., et al., Bright Triplet Excitons in Cesium Lead Halide Perovskites. *Nature.* **2018**, *553*, 189-195.
- S3. Kang, I.; Wise, F. W., Electronic Structure and Optical Properties of PbS and PbSe Quantum Dots. *J. Opt. Soc. Am. B.* **1997**, *14*, 1632-1646.

- S4. Hohenberg, P.; Kohn, W., Inhomogeneous Electron Gas. Phys Rev B. 1964, 136, 864-871.
- S5. Kohn, W.; Sham, L. J., Self-Consistent Equations Including Exchange and Correlation Effects. *Phys Rev.* **1965**, *140*, 1133-1138.
- S6. Perdew, J. P.; Burke, K.; Ernzerhof, M., Generalized Gradient Approximation Made Simple. *Phys. Rev. Lett.* **1996**, *77*, 3865-3868.
- S7. Qian, X.; Li, J.; Qi, L.; Wang, C. Z.; Chan, T. L., et al., Quasiatomic Orbitals for *ab initio* Tight-Binding Analysis. *Phys Rev B.* **2008**, *78*, 245112-245125.